Molecular Vision 2019; 25:517-526 <http://www.molvis.org/molvis/v25/517>
Received 13 December 2018 | Accepted 19 September 2019 | Published 21 September 2019

Ultrastructural variability of the juxtacanalicular tissue along the inner wall of Schlemm's canal

Elena Koudouna,[1] Robert D. Young,[1] Darryl R. Overby,[2] Morio Ueno,[3] Shigeru Kinoshita,[3] Carlo Knupp,[1] Andrew J. Quantock[1]

[1]Structural Biophysics Research Group, School of Optometry and Vision Sciences, Cardiff University, Wales, UK; [2]Department of Bioengineering, Imperial College London, London, UK; [3]Department of Ophthalmology, Kyoto Prefectural University of Medicine, Hirokoji Kawaramachi, Kamigyo-ku, Kyoto, Japan

Purpose: Increased resistance of aqueous humor drainage from the eye through Schlemm's canal (SC) is the basis for elevated intraocular pressure in glaucoma. Experimental evidence suggests that the bulk of outflow resistance lies in the vicinity of the inner wall endothelial lining of SC and the adjacent juxtacanalicular tissue (JCT). However, there is little understanding of how this resistance is generated, and a detailed understanding of the structure-function relationship of the outflow pathway has not been established yet. In the present study, regional variations in the ultrastructure of the JCT and the inner wall of SC were investigated in three dimensions.

Methods: With the use of serial block face scanning electron microscopy (SBF-SEM), the volume occupied by the electron lucent spaces of the JCT compared to that occupied by the cellular and extracellular matrix was investigated and quantified. The distribution of giant vacuoles (GVs) and pores in the inner wall endothelium of SC was further examined.

Results: With increasing distance from the inner wall of SC, the volume of the electron lucent spaces increased above 30%. In contrast, the volume of these spaces in immediate contact with the inner wall endothelium was minimal (<10%). Circumferential variability in the type and distribution of GVs was observed, and the percentage of GVs with pores varied between 3% and 27%.

Conclusions: These studies provide a detailed quantitative analysis of the ultrastructure of JCT and the distribution of GVs along the circumference of SC in three dimensions, supporting the non-uniform or segmental aqueous outflow.

Elevated intraocular pressure (IOP) associated with primary open-angle glaucoma is caused by increased aqueous humor outflow resistance [1-3]. While the bulk of outflow resistance lies near the downstream end of the trabecular meshwork (TM) and the inner wall endothelium of Schlemm's canal (SC) [4-8], there is little understanding of how this resistance is generated, or why this resistance becomes elevated in glaucoma. Understanding the mechanism of resistance generation, therefore, may inform novel approaches to target the mechanisms of outflow resistance generation as a means of reducing IOP in glaucoma.

The inner wall endothelium of SC lies within a biomechanically demanding environment, where it experiences large cellular deformations because of the peculiar nature of aqueous humor flow across the endothelium [9]. Because the flow passes in the basal-to-apical direction across the inner wall, the pressure drop between the IOP and the episcleral venous pressure deforms the endothelial cells lining SC, causing them to form dome-like bulges known as giant vacuoles (GVs) [9-13]. GVs are often associated with pores, which are micron-sized openings through the endothelium. Pores may pass either through transcellular "I" pores or between individual SC cells, paracellular "B" pores [14-17]. GVs and pores together are believed to provide a channel for transendothelial flow [16-22]. Importantly, the number of pores is reduced in glaucomatous eyes [19,20], suggesting that impaired function of the SC barrier may contribute to outflow obstruction associated with glaucomatous ocular hypertension.

Pores on their own, however, are likely insufficient to generate a significant contribution to outflow resistance [23]. Simply put, there are too many SC pores such that their net contribution to the hydrodynamic resistance of the inner wall should be too low to explain the bulk of outflow resistance generation. However, because pores are the pathway for flow across an otherwise continuous endothelium containing tight junctions, pores (or the mouth of a GV associated with a pore) represent local choke points where aqueous humor must converge, or "funnel," to cross the inner wall [7,22-25]. According to the funneling model, extracellular matrix in the immediate vicinity of a pore or GV mouth would have a dominant effect on the generation of outflow resistance [22].

Correspondence to: Andrew J Quantock, Structural Biophysics Group, School of Optometry and Vision Sciences, Cardiff University, Maindy Road, Cardiff CF24 4HQ, Wales, UK; +44 (0)29 2087 5064 FAX: +44 (0)29 2087 4859; email: QuantockAJ@cf.ac.uk

Although several investigators have examined the matrix composition in the juxtacanalicular tissue (JCT) [26-30], and quantified open spaces [18,31-37], few investigators have examined the relationship between optically open spaces and pores or GV mouths. The complex three-dimensional (3D) structure of the extracellular matrix upstream of the pore and/or GV may affect outflow resistance generation via funneling, but the structure of this tissue varies with distance from the inner wall, transitioning from a relatively dense (yet discontinuous) inner wall basement membrane to relatively loose ECM in the JCT. It is difficult to capture the 3D structure of this tissue using conventional two-dimensional sections. In this study, we used serial block face scanning electron microscopy (SBF-SEM) to examine the 3D ultrastructure of the JCT surrounding the basal openings of GVs and pores in the inner wall endothelium of SC in post-mortem human eyes.

METHODS

Tissue processing: One ostensibly healthy eye of a 69-year-old female donor with no report of previous ocular disease was obtained from the Bristol Eye Bank. Time of death to enucleation was 18 h, after which the eye was held overnight at 4 °C in a moist sterile chamber, and placed in 4% paraformaldehyde fixative the following morning. Careful dissection of the TM was performed by one of the authors (MU, a glaucoma surgeon) after which the tissue was post-fixed in 2.5% glutaraldehyde in 0.1 M sodium cacodylate buffer (pH 7.2) for 3 h at room temperature. To increase the backscatter electron signal for SBF-SEM, the tissue was infiltrated with 1% osmium tetroxide containing 1.5% potassium ferricyanide in 0.1 M sodium cacodylate for 1 h, and 1% tannic acid for an additional hour. Specimens were then infiltrated and polymerized in Durcupan epoxy resin (Agar Scientific, Stansted, UK). This study was approved by the School of Optometry and Vision Sciences Research and Ethics committee at Cardiff University, UK. Experiments were conducted in accordance with the ethical principles that have their origin in the Declaration of Helsinki, the ARVO statement for the use of human subjects, including human material and data, in biomedical research and in line with the requirements of the UK Human Tissue Act.

Transmission electron microscopy: Following sample embedding, the tissue was first investigated with transmission electron microscopy. Initially, a preliminary histological analysis was performed by obtaining 0.3 µm thick sections using an Ultracut E ultramicrotome (Reichert-Jung, Vienna, Austria). Semithin sections were stained with 1% toluidine blue, and visualized under a Olympus BH-2 light microscope (Tokyo, Japan) to facilitate optimization of the plane of the section, and identification of a suitable area of interest (Figure 1A). Ultrathin, 100 nm thick sections were also cut, and investigated using a JEM 1010 transmission electron microscope (JEOL, Tokyo, Japan) operating at 80 kv. An 11-megapixel Orius SC1000 CCD camera (Gatan, Pleasanton, CA) was used to acquire images.

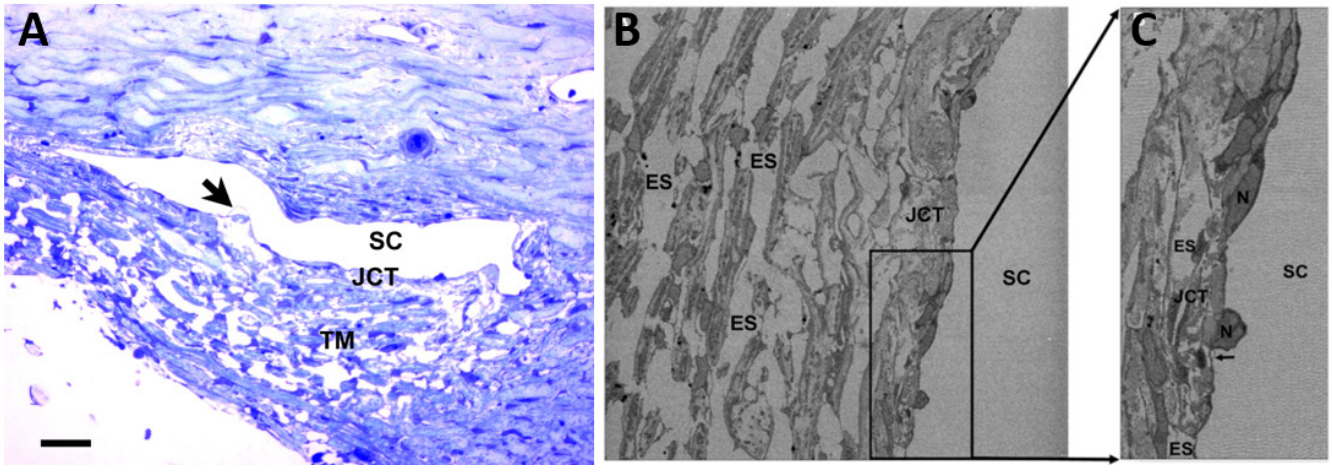

Figure 1. Serial block face scanning electron microscopy (SBF-SEM) of the human TM. **A**: Light microscopy of toluidine blue-stained meridional section through corneal limbus showing Schlemm's canal (SC), juxtacanalicular tissue (JCT), and trabecular meshwork (TM). A giant vacuole (GV, arrow) is visible on the inner wall of SC. Scale bar, 50 µm. **B**: SBF-SEM was conducted in a selected area of 4,096 × 4,096 pixels with magnification equating to 27 nm/pixel, and data sets of up to 500 images were acquired of the block face, renewed by successive slicing at 125 nm. An area of 1,588 × 1,844 pixels was selected for this study, shown in the boxed region. **C**: An isolated view of the boxed region shown in **B**. See also Appendix 1. SC = Schlemm's canal; JCT = Juxtacanalicular tissue; N = nucleus; ES = empty spaces.

Serial block face scanning electron microscopy: SBF-SEM was then performed using an FEI Quanta FEG 250 scanning electron microscope (Cambridge, UK) fitted with a Gatan 3View® system at the Wellcome Centre for Cell Matrix Research (Faculty of Life Science, University of Manchester, UK). Serial image data sets facilitated volume 3D reconstruction of the human TM nanostructure. The principle behind SBF-SEM is to repeatedly image the tissue block surface alternating with removal of a surface layer, in this case of 125 nm thickness, using a microtome located inside the microscope. A scan resolution of 4,096 × 4,096 pixels^2 (Figure 1B) with a magnification of 27 nm/pixel was employed in this study, entailing 500 serial backscatter electron images, at 125 nm intervals, that were collected at 3.8 kv, with a dwell time of 10 µs. The total area of the inner wall of SC analyzed in the present study was 3,170 µm^2. An area of 1,588 × 1,844 pixels^2 of the inner wall of SC and the JCT was selected for quantitative ultrastructural analysis in the present study (Figure 1C).

Quantitative ultrastructural analysis of the JCT and giant vacuoles: The volume occupied by the optically empty spaces of the JCT against the distance from the borders of SC was calculated to investigate the spatial variation under the inner wall of SC. Additionally, we sought to explore the spatial variation along the circumferential direction of SC. To achieve this, we evaluated the areal fraction occupied by optically empty spaces within the JCT at various locations along SC (12.5, 25, 37.5, 50, and 62.5 µm) referenced to the arbitrary starting position of the tissue block sectioning (Figure 2A). At each location, four micrographs were analyzed to determine the volume of the electron lucent spaces (excluding cellular and extracellular matrix components) as a function of distance from the inner wall of SC. To do this, we first identified the basal surface of the inner wall endothelium. This was traced and adjusted manually for each micrograph. Using a macro, we then divided the JCT into six parallel portions that were located 2.7, 5.4, 8.1, 10.8, 13.5, and 16.2 µm from the inner wall (Figure 2B). For each portion, we traced and measured the area of the electron lucent space, and normalized by the total area of the segment.

The borders of the inner wall of SC varied along the circumferential direction of the canal, and within the four micrographs examined at each distance under the inner wall. Therefore, the borders of the canal were traced and adjusted manually for every distance and every micrograph analyzed. A macro was used to create six segments that had a distance of 2.7, 5.4, 8.1, 10.8, 13.5, and 16.2 µm from the borders of the inner wall of SC. For every segment, the total volume of all the electron lucent spaces was determined by manually tracing around the perimeter of each space, calculating its area and then summing the areas. These data were normalized against the area of the box in the occasional cases where the box partially exceeded the edge of the micrograph. Area measurements were converted into volumes by multiplying by the thickness of the cut section (125 nm). The volume of the electron lucent space in the JCT, averaged across all four tissue regions examined and expressed as a percentage, was then plotted as a function of the distance from the inner wall of SC. GVs throughout the entire data set (500 serial micrographs; tissue depth 62.5 µm) were also analyzed to ascertain whether they contained pores, and whether they opened to the JCT or the SC, or both.

Three-dimensional reconstruction: Image processing, quantitative analysis, and 3D reconstructions were conducted with the use of Image J software package [38,39]. Selected sequences were presented in three dimensions using the 3D Viewer plugin of Image J.

Statistical analysis: The average volume occupied by the electron lucent spaces of the JCT at each distance upstream of the inner wall was used for statistical analysis using IBM SPSS Version 21.0 (SPSS Inc., Chicago, IL). The Shapiro-Wilk normality test, with $p>0.05$ showing normal distribution, was performed, followed by one-way ANOVA and the Holm-Sidak multiple comparisons test.

RESULTS

Ultrastructural analysis of the JCT: Transmission electron microscopy clearly identified the inner wall and lumen of Schlemm's canal, and the underlying JCT and corneoscleral TM (Figure 3). High-resolution analysis of the ultrastructure of the JCT, achieved with SBF-SEM, revealed structural differences as a function of distance from the inner wall of SC (Appendix 1). These structural differences reflected variations in the tissue proportion occupied by the electron lucent, optically empty spaces, compared to that by the TM cells and extracellular matrix components (Figure 3, Appendix 1).

To analyse quantitatively the relationship between the volume occupied by the optically empty spaces and the ultrastructure of the JCT along the canal's circumference, the data set was subdivided into 12.5 µm thick portions as described in the Methods section (Figure 2). This revealed no difference in the volume occupied by the electron lucent spaces of the JCT compared to that occupied by the cellular and extracellular matrix material as a function of the distance below the borders of SC. Moreover, a measure of the average volume of electron lucent spaces against the cellular and matrix material of the JCT at distances of 2.7, 5.4, 8.1, 10.8, 13.5, and 16.2 µm from the borders of the inner wall of SC was calculated (Figure 4). This showed that the percentage

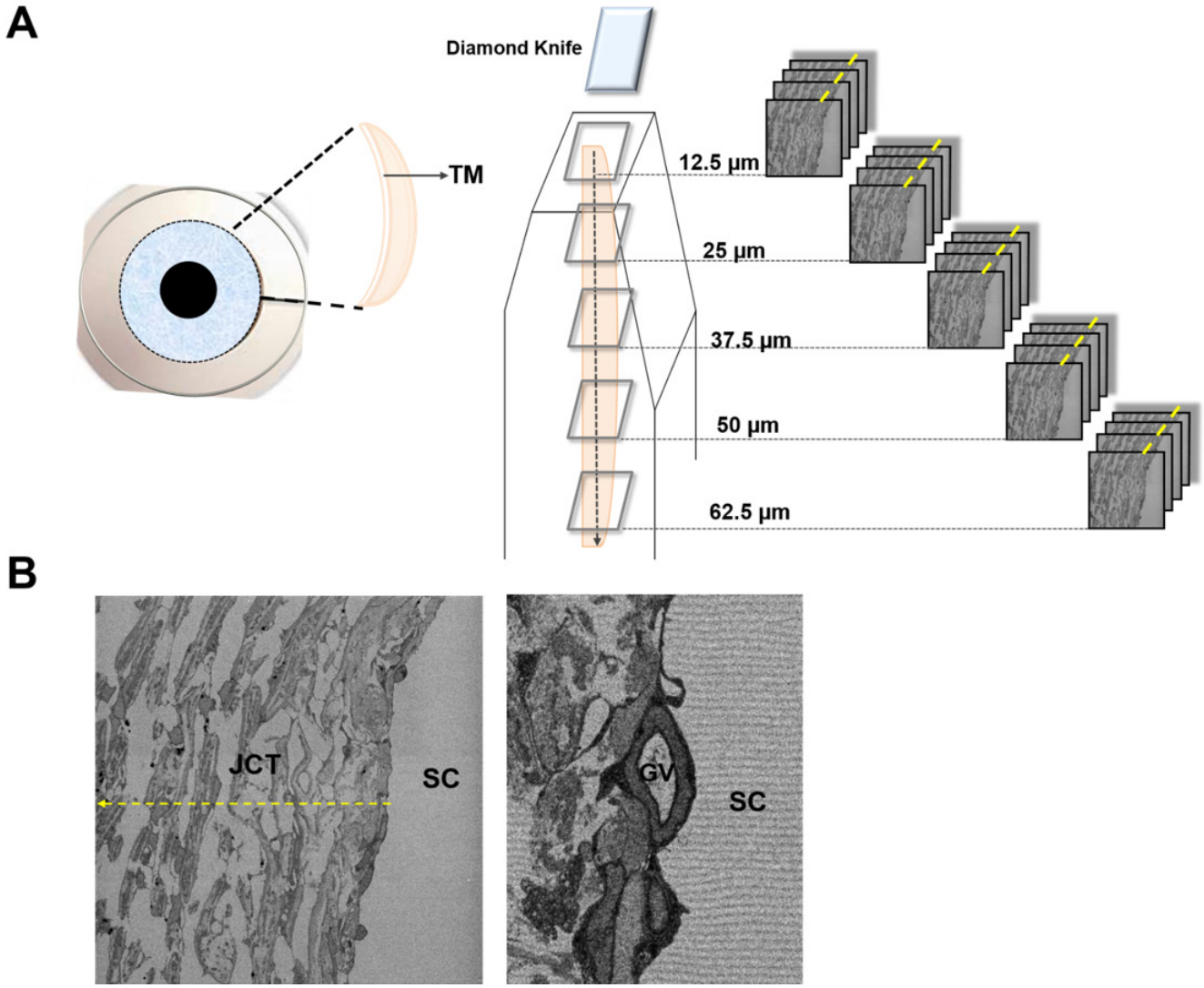

Figure 2. Diagrammatic representation of ultrastructural analysis of JCT and GV analysis along the circumference of SC. **A**: Human trabecular meshwork (TM) was dissected and embedded in resin for serial block face scanning electron microscopy (SBF-SEM). For purposes of this study, the data set was subdivided into four distinct regions (at 12.5, 25, 37.5, and 50 µm) starting from the initial block face. Each region consisted of 100 micrographs. **B**: Moving through the slices of the image stack, the borders of Schlemm's canal (SC) vary, and therefore, the borders of SC were always manually traced and adjusted within each slice within each of the four regions. A macro was then used to create six segments at a distance of 2.7, 5.4, 8.1, 10.8, 13.5, and 16.2 µm, upstream from the inner wall of SC (dotted line). The optically empty spaces within each of the six segments were manually traced, the perimeter was calculated, and the percentage of the volume occupied within each segment was determined.

of the volume occupied by the electron lucent spaces at a distance of 2.7 µm from the inner wall of SC was statistically significantly different (7.47±1.04%, $p<0.001$) compared to more distant regions. At a distance of 5.4 µm and 8.1 µm from the borders of the inner wall, the percentage of the volume occupied by the electron lucent spaces was 26.0±2.2% and 32.8±1.8%, respectively. While the volume occupied by the electron lucent spaces increased statistically significantly within the proximal 8.1 µm ($p<0.001$) from the inner wall of SC, thereafter the proportion of cellular and extracellular matrix components was enhanced, and therefore, a decrease in the volume of electron lucent spaces was noted. Farther away from the borders of SC, at a distance of 16.2 µm, the volume of electron lucent spaces of the JCT increased again to 33.0±5.0%, $p<0.001$.

Non-uniform distribution of GVs along the circumference of SC: GVs along the circumference of the inner wall of SC

Figure 3. Transmission electron microscopy of human TM. **A**: The endothelial lining of the inner wall of Schlemm's canal (SC) is indicated by the arrowheads. A giant vacuole (GV) is shown. **B**: The juxtacanalicular tissue (JCT) lies adjacent to the inner wall of SC and next to it the (**C**) trabecular meshwork (TM) beams are found. Scale bar=5 µm.

were counted and categorized into four types (Appendix 2), based on the endothelial vacuolation cycle as suggested by Tripathi [11]. A total of 40 GVs were tracked and manually segmented throughout the entire z-stack, a total of 500 serial micrographs. In one case, in which a GV was imaged at multiple slices throughout the z-stack and overlapped two SC circumference bins, the GV was excluded from analysis. Therefore, GVs were classified into four categories depending on whether the vacuoles exhibited: 1) no pores, or presented pores toward 2) the JCT region, 3) the lumen of SC, or 4) toward the JCT and SC (Figure 5A). The distribution and type of GV, however, were not evenly distributed throughout the entire circumference of the canal. In particular, a tissue depth of 12.5, 25, 37.5, 50, and 62.5 µm contained 27%, 8%, 22%, 8%, and 3% GVs with pores compared to the total GVs within each region, respectively (Figure 5B). Throughout the entire data set and a total tissue depth of 62.5 µm, the majority of the GVs had pores, toward either the JCT or the lumen of SC, or both (Figure 5C).

The type of GV, whether it had no pores, or pores opening toward the JCT, or the lumen of SC, or both, also appeared to vary within each region (Figure 5C). For instance, at 12.5 µm along the circumference of the canal, all four types of GV were present, whereas at 62.5 µm, only two types could be observed; GV with no pores and GV with pores toward the lumen of the canal.

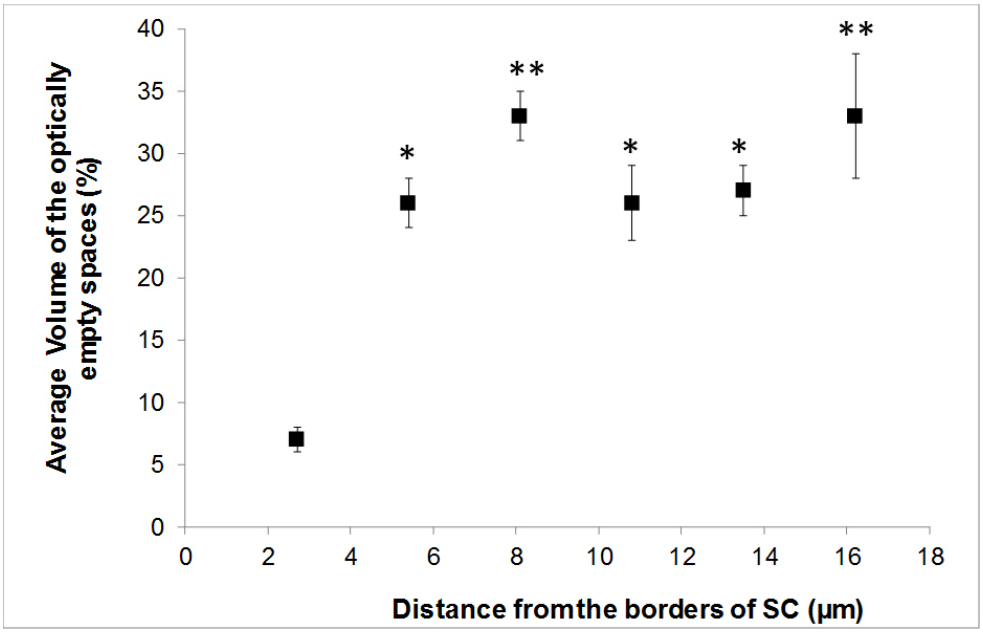

Figure 4. The volume occupied by the electron lucent spaces of the JCT is not uniform upstream of the inner wall of SC. The average volume, expressed as a percentage, occupied by the optically empty, electron lucent spaces of the juxtacanalicular tissue (JCT) against various distances from the borders of the inner wall of Schlemm's canal (SC). Error bars represent standard error. * $p<0.05$ when compared to 2.7 µm; ** $p<0.001$ when compared to 2.7 µm.

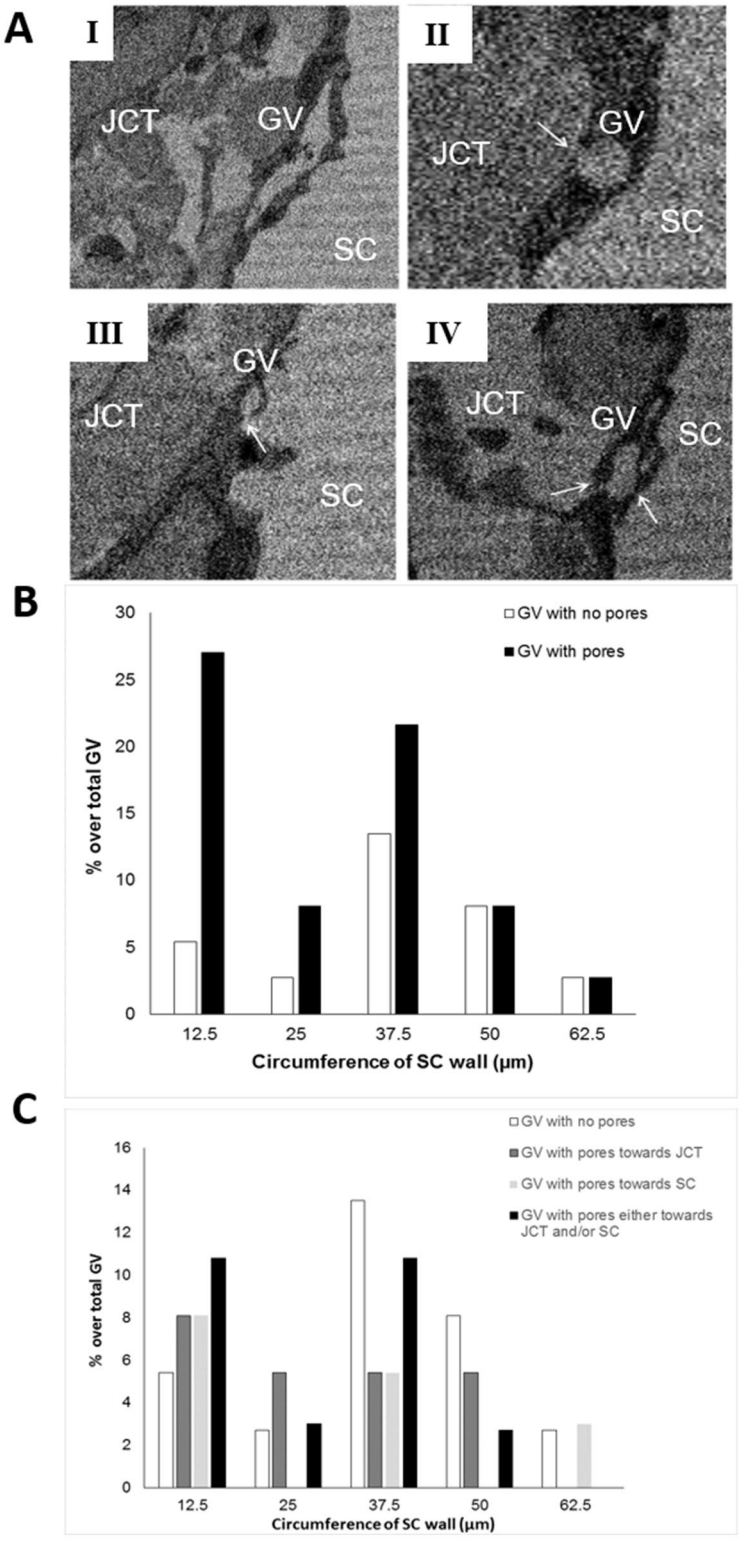

Figure 5. Non-uniform distribution of GVs across the circumference of the canal. **A**: Giant vacuoles (GVs) present at the endothelial cell lining of the inner wall of Schlemm's canal (SC). (I) A portion of the vacuoles did not possess any intracellular pores, while some of the vacuoles had pores opening (II) toward the juxtacanalicular tissue (JCT), (III) or toward the lumen of the canal (IV), or toward the JCT and SC. White arrows indicate the apical and basal pores. **B**, **C**: The type and distribution of GVs are non-uniform along the circumference of SC.

DISCUSSION

The predominant drainage pathway for aqueous humor is the conventional outflow pathway which consists of the TM, the JCT, the inner wall endothelium of SC, and the collector channels/aqueous veins [2,8,22,23]. Within the conventional outflow route of aqueous humor drainage, the bulk of outflow resistance is generated by the endothelial lining of SC and the adjacent JCT [6-8,40-42]. The funneling model has emerged as a hydrodynamic model that supports a synergistic outflow resistance generation in which pores in the inner wall [22], often associated with GVs, affect flow patterns in the conventional outflow route [37,43-48]. Yet, still unknown today are the specific mechanisms and the hydrodynamic details of how outflow resistance is generated and regulated. Despite numerous physiologic, pharmacological, and morphometric studies [49-55] a detailed understanding of the structure-function relationships of the outflow pathway, over large tissue volumes, has not been established. In this study, SBF-SEM was used to investigate a large area of the conventional outflow pathway, with a particular focus on the fine structure of the JCT and the GVs in the inner wall endothelium. Using this approach, a better characterization of regional variations in the ultrastructure of JCT was obtained, supporting the non-uniform or segmental aqueous outflow.

With the reported importance of the JCT in outflow resistance, numerous empirical studies calculated the amount of empty spaces or solid tissue within the JCT, in normal and glaucomatous tissues, including immersion- and perfusion-fixed samples [18,32,56-58]. Of these studies, the variability of the components of the JCT along the circumference of the JCT along the circumference of the eye was highlighted [18,32,56-58], emphasizing that large tissue specimen examination and sample size are crucial. The present study used immersion fixation to prepare the tissue, because others have found that perfusion fixation can lead to an artificial increase in the inner wall pore density [15,58-62]. Moreover, Braakman and associates [17] recently indicated that immersion fixed samples preserve pores and GVs along the inner wall of SC.

This study exceeded the limitation of two dimensions, and by using SBF-SEM, a powerful technique which enables 3D visualization of large tissue volumes at high resolution, examined the relationship between the volume occupied by the optically empty, electron lucent spaces of the JCT and the distance upstream of the inner wall endothelium. With increasing distance from the inner wall of SC, the volume of the electron lucent spaces increased above 30%. In contrast, the volume of these spaces in immediate contact with the inner wall endothelium was minimal (<10%). In accordance with previous morphometric studies of the JCT [6-8,32], these data suggest that within the JCT, the region in close proximity to the inner wall of SC might be attributable to outflow resistance regeneration. Simply put, the volume of the electron lucent spaces further away from SC is too big to statistically significantly contribute to outflow resistance, unless these spaces contain an unobserved extracellular matrix gel [31]. These findings are also in agreement with an elegant study by Lütjen-Drecoll in 1973, which showed a positive correlation between the outflow facility and the area of the electron lucent spaces in the subendothelial region of SC [63]. This is additionally supported by previous theoretical studies which characterized the subendothelial region of the JCT as the “locus generis” of aqueous humor outflow resistance [64]. Of interest, the ultrastructure pattern of JCT is indistinguishable along the circumference of the canal, at least for up to a distance of 50 µm from the arbitrary starting point, examined in this study.

The fact that the subendothelial JCT region is nearly depleted by electron lucent spaces, and the volume of these spaces increases with increasing distance from the canal, is of particular significance. Variation in the volume occupied by the optically empty spaces across the JCT thickness aids the establishment of a segmental outflow which will impact the outflow facility. Therefore, it is reasonable to speculate that this specific tissue ultrastructure acts to increase outflow resistance in the subendothelial region of SC. This particular tissue ultrastructure may further provide a supportive barrier, preventing collapse of SC, caused by uncontrolled outflow. An advantage of this study is that the volume of the empty spaces was measured in three dimensions, as opposed to previous investigations that were limited in two-dimensional area measurements [32,56,57,63]. Although JCT morphometric volume measurements potentially provide excellent accuracy, data consolidation by future studies with bigger sample numbers is a must.

The second part of this study examined the type and distribution of GVs along the circumference of SC. Circumferential variability in the type and distribution of GVs was observed. Taking into consideration that GVs and pores associated with them are thought to represent areas of active fluid drainage, and have been proposed to form preferentially near collector channels [34], these data reinforce previous experimental evidence supporting that aqueous flow is not evenly distributed throughout the inner wall [17,65-67]. Although the exact mechanism that drives the formation of GVs and pores is not well understood, biomechanical strain [16,17] and pressure drop across the inner wall have been implicated as underlying factors [11,15,19,21,68]. In a recent study, Lai and

colleagues, using SBF-SEM demonstrated that a decrease in cellular connectivity in the inner wall and JCT is associated with larger GV formation [62].

Taken together, these studies provide a detailed quantitative analysis of the ultrastructure of JCT and distribution of GVs along the circumference of SC. To the authors' knowledge, this correlation between the volume occupied by the electron lucent spaces and the distance upstream of the inner wall provides the first evidence from 3D observations, in our attempts to understand tissue-structure function relationships with respect to aqueous flow across the JCT. Although this study is preliminary, these findings are sufficiently promising to merit further development. Taking into account the variability among human eyes, future work with larger samples is necessary. Clearly understanding the cellular, molecular, and mechanical mechanisms that regulate aqueous outflow, in combination with changes in tissue-specific ultrastructure in health and disease, could accelerate our ability to devise more specific future glaucoma therapies. The opportunity offered by SBF-SEM in studying large tissue volumes at high resolution is highlighted in the present study, revealing the 3D ultrastructure within the TM. We believe this approach will be invaluable in future work to study the conventional aqueous humor outflow pathway in three dimensions in health and disease.

APPENDIX 1. SUPPLEMENTARY VIDEO 1.

To access the data, click or select the words "Appendix 1."

APPENDIX 2. SUPPLEMENTARY VIDEO 2.

To access the data, click or select the words "Appendix 2."

ACKNOWLEDGMENTS

Supported by a Cardiff University Professor Sir Martin Evans' President's Studentship to EK, by a BBSRC Project Grant (BB/M025349/1) to AJQ, CK, and RDY, and by collaborative research grants from the Japan Society for the Promotion of Sciences and the Japan Eye Bank.

REFERENCES

1. Gordon MO, Beiser JA, Brandt JD, Heuer DK, Higginbotham EJ, Johnson CA, Keltner JL, Miller JP, Parrish RK 2nd. Wilson MR, Kass MA. The ocular hypertension treatment study: baseline factors that predict the onset of primary open-angle glaucoma. Arch Ophthalmol 2002; 120:714-20. , discussion 829–30.. [PMID: 12049575].

2. Grant WM. Clinical measurements of aqueous outflow. Am J Ophthalmol 1951; 34:1603-5. [PMID: 14885362].

3. Grierson I, Lee WR. The fine structure of the trabecular meshwork at graded levels of intraocular pressure. (1) Pressure effects within the near-physiological range (8–30 mm Hg). Exp Eye Res 1975; 20:505-21. [PMID: 1149832].

4. Inomata H, Bill A, Smelser GK. Aqueous humor pathways through the trabecular meshwork and into Schlemm's canal in the cynomolgus monkey (Macaca irus). An electron microscopic study. Am J Ophthalmol 1972; 73:760-89. [PMID: 4623937].

5. Johnson M, Johnson DH, Kamm RD, DeKater AW, Epstein DL. The filtration characteristics of the aqueous outflow system. Exp Eye Res 1990; 50:407-18. [PMID: 2338123].

6. Lütjen-Drecoll E. Structural Factors Influencing Outflow Facility and its Changeability Under Drugs A Study in Macaca Arctoides. Invest Ophthalmol Vis Sci 1973; 12:280-94. [PMID: 4144361].

7. Mäepea O, Bill A. Pressures in the juxtacanalicular tissue and Schlemm's canal in monkeys. Exp Eye Res 1992; 54:879-83. [PMID: 1521580].

8. Overby DR, Stamer WD, Johnson M. The changing paradigm of outflow resistance generation: towards synergistic models of the JCT and inner wall endothelium. Exp Eye Res 2009; 88:656-70. [PMID: 19103197].

9. Holmberg AS. The fine structure of the inner wall of Schlemm's canal. Arch Ophthalmol 1959; 62:956-8. .

10. Johnstone MA, Grant WM. Pressure dependent changes in structures of the aqueous outflow system of human and monkey eyes. Am J Ophthalmol 1973; 75:365-83. [PMID: 4633234].

11. Tripathi RC. Aqueous outflow pathway in normal and glaucomatous eyes. Br J Ophthalmol 1972; 56:157-74. [PMID: 4113454].

12. Tripathi RC. Mechanism of the aqueous outflow across the trabecular wall of Schlemm's canal. Exp Eye Res 1971; 11:116-21. [PMID: 4108660].

13. Tripathi RC. The functional morphology of the outflow systems of ocular and cerebrospinal fluids. Exp Eye Res 1977; 25:65-116. [PMID: 590403].

14. Epstein DL, Rohen JW. Morphology of the trabecular meshwork and inner-wall endothelium after cationized ferritin perfusion in the monkey eye. Invest Ophthalmol Vis Sci 1991; 32:160-71. [PMID: 1987099].

15. Ethier CR, Coloma FM, Sit AJ, Johnson MC. Two pore types in the inner-wall endothelium of Schlemm's canal. Invest Ophthalmol Vis Sci 1998; 39:2041-8. [PMID: 9761282].

16. Braakman ST, Pedrigi RM, Read AT, Smith JAE, Stamer WD, Ethier CR, Overby DR. Biomechanical strain as a trigger for pore formation in Schlemm's canal endothelial cells. Exp Eye Res 2014; 127:224-35. [PMID: 25128579].

17. Braakman ST. A. Thomas Read, Darren W.-H. Chan, C. Ross Ethier, Darryl R. Overby. Colocalization of Outflow Segmentation and Pores Along the Inner Wall of Schlemm's Canal. Exp Eye Res 2015; 130:87-96. [PMID: 25450060].

18. Gong H, Ruberti J, Overby D, Johnson M, Freddo T. A new view of the human trabecular meshwork using quick-freeze, deep-etch electron microscopy. Exp Eye Res 2002; 75:347-58. [PMID: 12384097].
19. Allingham RR, de Kater AW, Ethier CR, Anderson PJ, Hertzmark E, Epstein DL. The relationship between pore density and outflow facility in human eyes. Invest Ophthalmol Vis Sci 1992; 33:1661-9. [PMID: 1559766].
20. Johnson M, Chan DWH, Read AT, Christensen C, Sit AJ, Ethier CR. The pore density in the inner wall endothelium of Schlemm's canal of glaucomatous eyes. Invest Ophthalmol Vis Sci 2002; 43:2950-5. [PMID: 12202514].
21. Pedrigi RM, Simon D, Reed A, Stamer WD, Overby DR. A model of giant vacuole dynamics in human Schlemm's canal endothelial cells. Exp Eye Res 2011; 92:57-66. [PMID: 21075103].
22. Johnson M, Shapiro A, Ethier CR, Kamm RD. Modulation of outflow resistance by the pores of the inner wall endothelium. Invest Ophthalmol Vis Sci 1992; 33:1670-5. [PMID: 1559767].
23. Bill A, Svedbergh B. Scanning electron microscopic studies of the trabecular meshwork and the canal of Schlemm – An attempt to localize the main resistance to outflow of aqueous humor in man. Acta Ophthalmol 1972; 50:295-320. [PMID: 4678226].
24. Stamer WD, Acott TS. Current understanding of conventional outflow dysfunction in glaucoma. Curr Opin Ophthalmol 2012; 23:135-43. [PMID: 22262082].
25. Tamm ER. The trabecular meshwork outflow pathways: Structural and functional aspects. Exp Eye Res 2009; 88:648-55. [PMID: 19239914].
26. Acott TS, Kelley MJ. Extracellular matrix in the trabecular meshwork. Exp Eye Res 2008; 86:543-61. [PMID: 18313051].
27. Keller KE, Aga M, Bradley JM, Kelley MJ, Acott TS. Extracellular matrix turnover and outflow resistance. Exp Eye Res 2009; 88:676-82. [PMID: 19087875].
28. Tawara A, Varner HH, Hollyfield JG. Distribution and characterization of sulfated proteoglycans in the human trabecular tissue. Invest Ophthalmol Vis Sci 1989; 30:2215-31. [PMID: 2793361].
29. Gonzalez JM, Hamm-Alvarez S, Tan JCH. Analysing live cellularity in the human trabecular meshwork. Invest Ophthalmol Vis Sci 2013; 54:1039-47. [PMID: 23249706].
30. Gonzalez JM, Heur M, Tan JCA. Two-photon immunofluorescence characterization of the trabecular meshwork in situ. Invest Ophthalmol Vis Sci 2012; 53:3395-404. [PMID: 22531697].
31. Ethier CR, Kamm RD, Palaszewski BA, Johnson M, Richardson TM. Calculations of flow resistance in the juxtacanalicular meshwork. Invest Ophthalmol Vis Sci 1986; 27:1741-50. [PMID: 3793404].
32. Buller C, Johnson D. Segmental variability of the trabecular meshwork in normal and glaucomatous eyes. Invest Ophthalmol Vis Sci 1994; 35:3841-51. [PMID: 7928181].
33. Brilakis HS, Hann CR, Johnson DH. A comparison of different embedding media on the ultrastructure of the trabecular meshwork. Curr Eye Res 2001; 22:235-44. [PMID: 11462161].
34. Parc CE, Johnson DH, Brilakis HS. Giant vacuoles are found preferentially near collector channels. Invest Ophthalmol Vis Sci 2000; 41:2984-90. [PMID: 10967055].
35. Chu ER, Gonzalez JM, Tan JCH. Tissue-based imaging model of human trabecular meshwork. J Ocul Pharmacol Ther 2014; 30:191-201. [PMID: 24517246].
36. Gottanka J, Chan D, Eichhorn M, Lütjen-Drecoll E, Ethier CR. Effects of TGF-beta2 in perfused human eyes. Invest Ophthalmol Vis Sci 2004; 45:153-8. [PMID: 14691167].
37. Johnson DH. The effect of cytochalasin D on outflow facility and the trabecular meshwork of the human eye in perfusion organ culture. Invest Ophthalmol Vis Sci 1997; 38:2790-9. [PMID: 9418732].
38. Schmid B, Schindelin J, Cardona A, Longair M, Heisenberg M. A high-level 3D visualization API for Java and ImageJ. BMC Bioinformatics 2010; 11:1471-2105. [PMID: 20492697].
39. Schneider CA, Rasband WS, Eliceiri KW. NIH Image to ImageJ: 25 years of image analysis. Nat Methods 2012; 9:671-5. [PMID: 22930834].
40. Johnson M, Chan D, Read AT, Christensen C, Sit A, Ethier CR. The pore density in the inner wall endothelium of Schlemm's canal of glaucomatous eyes. Invest Ophthalmol Vis Sci 2002; 43:2950-5. [PMID: 12202514].
41. Rosenquist R, Epstein D, Melamed S, Johnson M, Grant WM. Outflow resistance of enucleated human eyes at two different perfusion pressures and different extents of trabeculotomy. Curr Eye Res 1989; 8:1233-40. [PMID: 2627793].
42. Moseley H, Grierson I, Lee WR. Mathematical modelling of aqueous humor outflow from the eye through the pores in the lining of Schlemm's canal. Clin Phys Physiol Meas 1983; 4:47-63. [PMID: 6831842].
43. Sabanay I, Gabelt BT, Tian B, Kaufman PL, Geiger B. H-7 effects on the structure and fluid conductance of monkey trabecular meshwork. Arch Opthalmol. 2000; 118:955-62. [PMID: 10900110].
44. Sabanay I, Tian B, Gabelt BT, Geiger B, Kaufman PL. Functional and structural reversibility of H-7 effects on the conventional aqueous outflow pathway in monkeys. Exp Eye Res 2004; 78:137-50. [PMID: 14667835].
45. Ethier CR, Read AT, Chan DW. Effects of latrunculin-B on outflow facility and trabecular meshwork structure in human eyes. Invest Ophthalmol Vis Sci 2006; 47:1991-8. [PMID: 16639007].
46. Grierson I, Lee WR, Moseley H, Abraham S. The trabecular wall of Schlemm's canal: A study of the effects of pilocarpine by scanning electron microscopy. Br J Ophthalmol 1979; 56:935-52. [PMID: 760777].
47. Svedbergh B. Protrusions of the inner wall of Schlemm's canal. Am J Ophthalmol 1976; 82:875-82. [PMID: 826163].

48. Chang JY, Folz SJ, Laryea SN, Overby DR. Multi-scale analysis of segmental outflow patterns in human trabecular meshwork with changing intraocular pressure. J Ocul Pharmacol Ther 2014; 30:213-23. [PMID: 24456518].

49. Bill A, Lütjen-Drecoll E, Svedbergh B. Effects of intracameral NA_2EDTA and EGTA on aqueous outflow routes in the monkey eye. Invest Ophthalmol Vis Sci 1980; 19:492-504. [PMID: 6768690].

50. Hamanaka T, Bill A. Morphological and functional effects of NA_2EDTA on the outflow routes for aqueous humor in monkeys. Exp Eye Res 1987; 44:171-90. [PMID: 3108020].

51. Hamanaka T, Bill A. Effects of alpha-chymotrypsin on the outflow routes for aqueous humor. Exp Eye Res 1988; 46:323-41. [PMID: 3350074].

52. Raghunathan V, Eaton JS, Christian BJ, Morgan JT, Ver Hoeve JN, Charlie Yang C-Y, Gong H, Rasmussen CA, Miller PE, Russell P, Nork TM, Murphy CJ. Biomechanical, ultrastructural, and electrophysiological characterization of the non-human primate experimental glaucoma model. Sci Rep 2017; 7:14329-[PMID: 29085025].

53. Ethier CR, Chan DW-H. Cationic ferritin changes outflow facility in human eyes whereas anionic ferritin does not. Invest Ophthalmol 2001; 42:1795-802. [PMID: 11431444].

54. Ethier CR, Read AT, Chan DWH. Biomechanics of Schlemm's Canal Endothelial Cells: Influence on F-Actin Architecture. Biophys J 2004; 87:2828-37. [PMID: 15454474].

55. McMenamin PG, Lee WR, Aitken DAN. Age-related changes in the human outflow apparatus. Ophthalmol. 1986; 93:194-209. [PMID: 3951826].

56. Ten Hulzen RD, Johnson DH. Effect of fixation pressure on juxtacanalicular tissue and Schlemm's canal. Invest Ophthalmol Vis Sci 1996; 37:114-24. [PMID: 8550315].

57. Hann CR, Bentley MD, Vercnocke A, Ritman EL, Fautsch MP. Imaging the human aqueous humor outflow pathway in human eyes by three dimensional micro-computed tomography (3D micro-CT). Exp Eye Res 2011; 92:104-11. [PMID: 21187085].

58. Sit AJ, Coloma FM, Ethier CR, Johnson MC. Factors affecting the pores of the inner wall endothelium of Schlemm's canal. Invest Ophthalmol Vis Sci 1997; 38:1517-25. [PMID: 9224279].

59. Lee WR, Grierson I. Pressure effects on the endothelium of the trabecular wall of Schlemm's canal: A study by scanning electron microscopy. Albrecht von Graefes Arch. Klin. Ophthalmol. 1975; 196:255-6. [PMID: 813538].

60. Grierson I, Lee WR. Pressure-induced changes in the ultrastructure of the endothelium lining Schlemm's canal. Am J Ophthalmol 1975; 80:863-84. [PMID: 811121].

61. Grierson I, Lee WR. Changes in the monkey outflow apparatus at graded levels of intraocular pressure: a qualitative analysis by light microscopy and scanning electron microscopy. Exp Eye Res 1974; 19:21-33. [PMID: 4412389].

62. Lai J, Su Y, Swain DL, Huang D, Getchevski D, Gong H. The role of Schlemm's canal and endothelium cellular connectivity in giant vacuole formation: a 3D electron microscopy study. Invest Ophthalmol Vis Sci 2019; 60:1630-43. [PMID: 30995299].

63. Lütjen-Drecoll E. Structural factors influencing outflow facility and its changeability under drugs. A study in Macaca arctoides. Invest Ophthalmol 1973; 12:280-94. [PMID: 4144361].

64. Seiler T, Wollensak J. The resistance of the trabecular meshwork to aqueous humor outflow. Graefes Arch Clin Exp Ophthalmol 1985; 223:88-91. [PMID: 4007511].

65. Hann CR, Fautsch MP. Preferential fluid flow in the human trabecular meshwork near collector channels. Invest Ophthalmol Vis Sci 2009; 50:1692-7. [PMID: 19060275].

66. Keller KE, Bradley JM, Vranka JA, Acott TS. Segmental versican expression in the trabecular meshwork and involvement in outflow facility. Invest Ophthalmol Vis Sci 2011; 52:5049-57. [PMID: 21596823].

67. Chang JY, Folz SJ, Laryea SN, Overby DR. Multi-scale analysis of segmental outflow patterns in human trabecular meshwork with changing intraocular pressure. J Ocul Pharmacol Ther 2014; 30:213-23. [PMID: 24456518].

68. Overby DR, Zhou EH, Vargas-Pinto R, Pedrigi RM, Fuchshofer R, Braakman ST, Gupta R, Perkumas KM, Sherwood JM, Vahabikashi A, Dang Q, Kim JH, Ethier CR, Stamer WD, Fredberg JJ, Johnson M. Altered mechanobiology of Schlemm's canal endothelial cells in glaucoma. Proc Natl Acad Sci USA 2014; 111:13876-1381. [PMID: 25201985].

Articles are provided courtesy of Emory University and the Zhongshan Ophthalmic Center, Sun Yat-sen University, P.R. China. The print version of this article was created on 21 September 2019. This reflects all typographical corrections and errata to the article through that date. Details of any changes may be found in the online version of the article.